Green-Emissive Ce^{3+}:$Lu_3Al_5O_{12}$-Al_2O_3 Nanoceramics Elaborated via Glass Crystallization for High-Power Laser Lighting Applications

Abstract

Transparent Ce:$Lu_3Al_5O_{12}$ (Ce:LuAG) phosphor ceramics are regarded as the most promising green color conversion materials in the next-generation of laser diode (LD) lighting. However, the insufficient absorption and conversion of blue laser and severe heat quenching seriously prevent the application of transparent Ce:LuAG phosphor ceramics in high-quality LD-driven lighting, especially under high input power density. In view of this, a biphasic Ce:LuAG-Al_2O_3 green phosphor ceramic is proposed in this study. Using an excessive Al_2O_3 component design strategy, the Al_2O_3 secondary phase is in-situ generated in the resulting ceramic material via the full bulk glass crystallization method. The in-situ generated Al_2O_3 secondary phase can serve as light scattering centers and has good thermal conductivity. Therefore, the luminescent properties and thermal stability of transparent Ce:LuAG-Al_2O_3 phosphor ceramics are greatly enhanced compared to Ce:LuAG. An ultrahigh luminous flux (LF) of 5,125 lm and an excellent luminous density of 4235.5 $lm \cdot mm^{-2}$ are achieved in LD-driven lighting under 450 nm high power density laser excitation (29.83 $W \cdot mm^{-2}$), which is almost the best performance of transparent Ce:LuAG ceramics in LD lighting to date. A maximum luminous efficiency of 247.9 $lm \cdot W^{-1}$ (4.38 $W \cdot mm^{-2}$) is also obtained. These results demonstrate that the transparent Ce:LuAG-Al_2O_3 nanoceramics prepared in this work are promising green-emitting color converters in order to achieve high-brightness and excellent luminous density for high power LD lighting. The excessive Al_2O_3 component design strategy could also further drive the development of garnet-based transparent ceramics in the field of high-power LD lighting.

1. Introduction

Solid state lighting (SSL) technology represented by light emitting diodes (LEDs) has been widely applied in modern lighting and backlight displays.[1-3] LEDs have many

advantages such as high brightness, long lifespan, energy conservation, and environmental protection.[4] However, LEDs have an inherent problem of "efficiency droop" at high input power density, which is not caused by thermal effects.[5] This limits the widespread applications of LEDs in high-power electricity-to-light converter devices. On the contrary, laser diodes (LDs) do not exhibit the above issues of "efficiency droop" and can achieve extremely high brightness luminescence at high input power density.[6-9] Moreover, lasers have good collimation and can easily focus on an area with a diameter of several millimeters.[10] Therefore, LDs are considered as the next generation of lighting technology for scenarios requiring high brightness, fast response, and long-distance lighting.

Recently, it was reported that under LD excitation, yellow/green/red color converters can achieve high-quality white lighting with rich spectral components.[11-15] Thus, the light conversion efficiency and thermal stability of color converters become the key parameter to maintain high output power and good reliability at high input power density.[16] Color converters usually generate a large amount of heat due to the excitation of high power input laser, and the temperature of the device rapidly increases.[17-20] This poses a huge challenge to the heat resistance of color converters. Conventional powder phosphors are often encapsulated in organic compounds[21], but for high power LD, the organic color converters have poor thermal resistance and are quickly destroyed and become ineffective. Therefore, novel full inorganic color converters with high thermal conductivity have emerged. These full inorganic color converters have good thermal performance and can withstand high power incident lasers well. These novel full inorganic color converters mainly include three categories, i.e. phosphor-in-glass (PiG)/glass ceramics[22-23], single crystals[24-25], and transparent ceramics[26-28]. Due to their low thermal conductivity (1-3 $W \cdot m^{-1} \cdot K^{-1}$), the luminescence performances of PiG/glass ceramics decrease under long-term excitation of high-power input laser, which affects the service life of electricity-to-light converter devices.[29] Single crystals have good optical and thermal properties, but their low doping concentration, complex and costly preparation

process, restricted size, and especially the inability to customize the scattering centers, result in a large amount of input laser excitation not being captured and converted, and thus these materials are incapable to achieve high luminous efficiency.[30] Transparent ceramics possess the comprehensive advantages of the aforementioned materials, including excellent transmittance, high mechanical properties, good thermal stability, high doping concentration, and controllable microstructure.[31-33] Therefore, transparent ceramics became a very suitable choice for high-power LD lighting.

For green phosphor ceramics, transparent Ce:YAG ceramics have been widely used in LEDs due to their excellent quantum efficiency and chemical stability.[34-35] However, serious thermal quenching limits the application of transparent Ce:YAG ceramics in high power LD lighting.[36] Compared to transparent Ce:YAG ceramics, Ce:LuAG transparent ceramics are more suitable for high power LD lighting due to higher luminous efficiency, lower thermal quenching property, and better quantum efficiency.[37] In recent years, there have been some reports on transparent Ce:LuAG ceramics being used as green color converters for LD lighting.[37-38] However, due to the lack of scattering centers, the blue laser easily passes directly through the transparent Ce:LuAG ceramics, reducing the absorption and conversion efficiency of blue laser, resulting in low luminous efficiency and affecting their application in high power LD lighting. Therefore, one important issue of transparent Ce:LuAG ceramics as green color converters for high power LD lighting applications is to provide scattering centers and enhance the luminous efficiency. In order to prepare green color converters with high brightness and high luminous efficiency under the excitation of high power LD, researchers have considered to introduce some scattering centers into transparent Ce:LuAG ceramics including CaF_2, $MgAl_2O_4$, AlN, and Al_2O_3 particles.[39-41] It was also demonstrated that residual micropores are interesting to ensure light scattering. Within these possibilities, Al_2O_3 crystal phase possesses excellent thermal conductivity and high transmittance in the visible region, making it an interesting candidate to be introduced as a secondary phase into transparent Ce:LuAG ceramics. However, introducing external scattering centers into a

transparent ceramic matrix (after the synthesis of ceramic nano-powders, before high-temperature sintering) has drawbacks: this approach will reduce the densification of the transparent ceramic matrix, and the dispersion of the introduced external scattering centers is uneven.[42] Therefore, if the Al_2O_3 secondary phase can be generated in situ in transparent Ce:LuAG ceramics, not only scattering centers will be successfully generated, but also densification limitations and heterogeneous phase dispersion will be avoided. So far, there are no reports on the preparation of Ce:LuAG based transparent phosphor ceramics with in-situ generated Al_2O_3 secondary phase as light scattering centers for high power LD lighting.

In this work, new biphasic transparent Ce:LuAG-Al_2O_3 nanoceramics were successfully prepared using an excessive Al_2O_3 component design strategy via a full bulk glass-crystallization method. The glass-crystallization method is a recent innovative approach which has enabled the preparation of new transparent ceramics in recent years. Using this process, an amorphous glass can be crystallized into transparent nanoceramics at relatively low temperature (≤ 1200 ℃) and a short time (<10 h).[43] The in-situ generated Al_2O_3 secondary phase in transparent Ce:LuAG-Al_2O_3 nanoceramics shows good thermal stability and can serve as light scattering centers. The biphasic transparent Ce:LuAG-Al_2O_3 ceramics with nanoscale grains exhibit a biphasic three-dimensional network nanostructure, in which the in-situ generated Al_2O_3 secondary phase is uniformly dispersed in the LuAG main phase and strongly scatters the incident blue laser to generate highly uniform green light. An ultrahigh luminous flux of 5,125 lm and an excellent luminous density of 4235.5 $lm \cdot mm^{-2}$ were achieved in LD-driven green lighting under 450 nm high-power density laser excitation (29.83 $W \cdot mm^{-2}$) by using transparent Ce:LuAG-Al_2O_3 nanoceramics in a reflection mode. Moreover, under a laser excitation of 4.38 $W \cdot mm^{-2}$, a maximum luminous efficiency of 247.9 $lm \cdot W^{-1}$ was also obtained. We believe that the transparent Ce:LuAG-Al_2O_3 nanoceramics are promising green-emitting color converters for high-power, LD-driven high-brightness solid-state lighting.

2. Experimental Section

2.1. Sample Preparation

High-purity commercial oxide powders Al_2O_3, CeO_2 (99.99%, Sinopharm chemical reagent co. ltd) and Lu_2O_3 (99.99%, Qiandong Rare Earth Group Co. Ltd) were used as starting materials. The starting material powders were weighed according to the composition of 72 mol.% Al_2O_3-28 mol.% ((1-x)Lu_2O_3, 2xCeO_2), (x=0, 0.003), and mixed in an agate mortar using ethanol as a dispersant, then dried at 50 °C in an air drying oven. The above steps were repeated 3 times. The mixed powders of 2-5 g were pressed into pellets, broken into 0.05-0.1 g fragments, and placed in an aerodynamic levitation furnace coupled with CO_2 laser heating. The fragments were heated and melted at ~2800 °C and levitated for 10-30 s followed by rapid quenching with a cooling rate of ~350 K/s by turning off laser heating, then transparent glass beads were fabricated. The transparent glass beads were crystallized at 950-1300 ℃ for 2 hours to prepared transparent ceramics.

2.2. Sample Characterization

Photoluminescence excitation (PLE) spectra, photoluminescence (PL) spectra, and fluorescence decay curves of samples were measured by the fluorescence spectrometer (FluoroMax Plus, Horiba, America). The integrating sphere fluorescence spectrometer (QE-2100, Otsuka Photal Electronics, Japan) was used to acquire quantum efficiency of samples. X-ray powder diffraction (XRPD, Smartlab 9, Rigaku Corporation, Japan) with Cu-Ka radiation was used to measure and analyze the crystalline phases and their structure, as well as crystallite sizes. XRPD results were analyzed by the Rietveld method using the full spectrum fitting (the least squares method was used for fitting) and a strain correction factor was also added to correct the obtained crystallite sizes. The in-line transmittance of samples (1.0 mm thickness) was recorded through a UV-VIS-NIR spectrophotometer (Cary 5000, Agilent Inc., USA) and a Fourier-transform infrared spectrometer (Excalibur 3100, Varian Inc., USA), with testing wavelength ranges of 190-2500 nm and 2500~7000 nm, respectively. Scanning electron microscopy (SEM, JSM-7001F, JEOL, Japan) was

used to record backscattered patterns of the ceramic samples. Transmission electron microscopy (TEM) was used to characterize the nanostructures of the ceramic samples, including HRTEM and STEM-HAADF imaging modes and EDX elemental analyzes (line-scan and mapping). These experiments were performed on a ARM200 Cold FEG microscope (JEOL Ltd) operating at 200kV, equipped with a JEOL SDD CENTURIO EDS system and fitted with a double spherical aberration corrector. The transparent ceramics were first prepared by mechanical polishing with a polishing machine to reach a thickness of 40 μm and then argon ion milling (Gatan PIPS) was used to prepare thin foils. The light scattering properties of ceramic samples were analyzed through a confocal laser scanning microscope (CLSM; Leica SP8 STED 3X, Leica Micromanipulator, Mannheim, Germany), a 470 nm argon laser was equipped as the excitation source and the image was acquired in confocal mode. The luminescent properties of ceramic samples, including electroluminescence (EL) spectra, absorption efficiency (Abs.), internal efficiency (IE), luminous efficiency (LE), color coordinates (CIE), luminous flux (LF) and luminous density, were measured by an optical testing system. This optical testing system includes high-power blue laser sources (450 nm), an integrating sphere (PMS-50, Everfine, Hangzhou, China) and a multichannel spectrometer (F-4600, Hitachi, Chengdu, Japan). The current, voltage, spot area, and power density of the high-power blue laser sources are 0.06-3.0 A, 0.565-54.2 W, 1.21 mm^2 and 0.47-44.79 $W \cdot mm^{-2}$, respectively.

3. Results and discussion

Figure 1(a) shows the preparation process of transparent Ce:LuAG-Al_2O_3 nanoceramics via full bulk glass crystallization at different temperature. **Figure 1(b,c)** present the photoluminescence excitation (PLE) and emission (PL) spectra of transparent Ce:LuAG-Al_2O_3 nanoceramics obtained at different temperature. It can be seen from **Figure 1(b)** that all Ce:LuAG-Al_2O_3 nanoceramics exhibit two typical broadband excitation peaks located around 450 nm and 350 nm, corresponding to the $4f \rightarrow 5d_1$ and $4f \rightarrow 5d_2$ level transitions of Ce^{3+}, respectively. The emission spectra in

Figure 1(c) show that all Ce:LuAG-Al_2O_3 nanoceramics exhibit a narrow emission spectrum with a peak around 510 nm and FWHM of 80 nm under the excitation wavelength of 450 nm, corresponding to the $5d_1 \rightarrow 4f$ transition of Ce^{3+}. Therefore, Ce:LuAG-Al_2O_3 nanoceramics can well absorb blue light with a wavelength of about 450 nm, and emit green light with a wavelength of about 510 nm. The maximum PLE and PL signals are observed when the crystallization temperature is 1200 ℃. As shown in the normalized PL spectrum **(Figure S1)**, the emission peak position does not show a significant change with the increase of crystallization temperature. The emission wavelength of Ce^{3+} is mainly affected by the separation degree of the 4f-5d and the splitting of the coordination field of the 5d level. However, in this single group of Ce:LuAG-Al_2O_3 nanoceramics, the separation degree of the 4f-5d remains approximately constant, thus the splitting of the coordination field of the 5d level plays a prominent role.[44] When the crystallization temperature gradually increases from 1100 ℃ to 1300 ℃, the grain size **(Figure S2)** gradually increases accordingly, while the position of the PL emission peak remains almost constant, which indicates that the coordination field of the 5d level of Ce^{3+} in the Ce:LuAG-Al_2O_3 nanoceramics has hardly changed with the increase of temperature. Taking advantage of this feature, Ce:LuAG-Al_2O_3 nanoceramics can be excited by high power blue LD for solid-state green lighting and display. **Figure 1(d)** and **Figure 1(e)** show the corresponding CIE coordinates of the Ce:LuAG-Al_2O_3 nanoceramics obtained at different crystallization temperatures. As the crystallization temperature increases, the coordinates of Ce:LuAG-Al_2O_3 nanoceramics gradually move towards the edge of the CIE figure, and then gradually move away from the edge. When the crystallization temperature reaches 1200 ℃, the coordinates of the nanoceramics are closest to the edge, indicating that the sample has the highest color saturation (color purity) at this crystallization temperature.[45]

Figure 1(f) shows the quantum efficiency (QE) of transparent Ce:LuAG-Al_2O_3 nanoceramics crystallized at different temperatures. It can be seen that the quantum efficiency of Ce:LuAG-Al_2O_3 nanoceramics first increases and then decreases with

the increase of crystallization temperature, and crystallization temperature of 1200 ℃ is the inflection point. When the excitation wavelength is 450 nm, the Ce:LuAG-Al_2O_3 nanoceramic crystallized at 1200 ℃ has the maximum quantum efficiency of 89.6%. The photographs of nanoceramics crystallized at different temperatures are presented in the bottom inset. It can be seen that the transmittance of Ce:LuAG-Al_2O_3 nanoceramics gradually decreases with the increase of crystallization temperature. However, the grain size of nanoceramics gradually increases with the increase of crystallization temperature, as shown in **Figure 2**. The quantum efficiency of transparent Ce:LuAG-Al_2O_3 nanoceramics is related to the transmittance and grain development of these nanoceramics. When the crystallization temperature is 1200 ℃, the transmittance and grain development of the nanoceramics achieve the best synergistic effect, thus obtaining the highest QE. Xu et al.[46] coated Ce:$Lu_3Al_5O_{12}$ phosphor grains with SiO_2 shell, and then co-sintered them with Na_2O-CaO-Al_2O_3-SiO_2 glass, the quantum efficiency of the obtained phosphor glass-ceramic was only 59%. Therefore, compared with phosphor glass-ceramic, the quantum efficiency of these transparent Ce:LuAG-Al_2O_3 nanoceramics has a significant advantage, and is also slightly higher than that of Ce:LuAG single-phase transparent ceramics (85.5%).[47]

The fluorescent decay curves of transparent Ce:LuAG-Al_2O_3 nanoceramics crystallized at different temperatures are shown in **Figure 1(g)** and the decay times can be obtained by single exponential fitting. The decay curves were recorded by monitoring the decay behavior of the Ce^{3+} emission peak at 510 nm under excitation at 450 nm wavelength. These decay curves were fitted with a single exponential decay equation as follows:

$$I = \mathrm{A}\exp\left(-\frac{t}{\tau}\right) + I_0$$

where I is the fluorescence intensity, t is the time, τ is the fluorescence lifetime, A and I_0 are constants. The results show that the decay behavior of Ce^{3+} at 510 nm in all Ce:LuAG-Al_2O_3 nanoceramics conforms to a single exponential decay with a decay time of about 57 ns. This is consistent with the fluorescence decay time of most Ce^{3+}

doped garnet transparent ceramics.[48] Fast decay is beneficial to avoid "luminescence saturation" phenomenon under high power density light excitation.

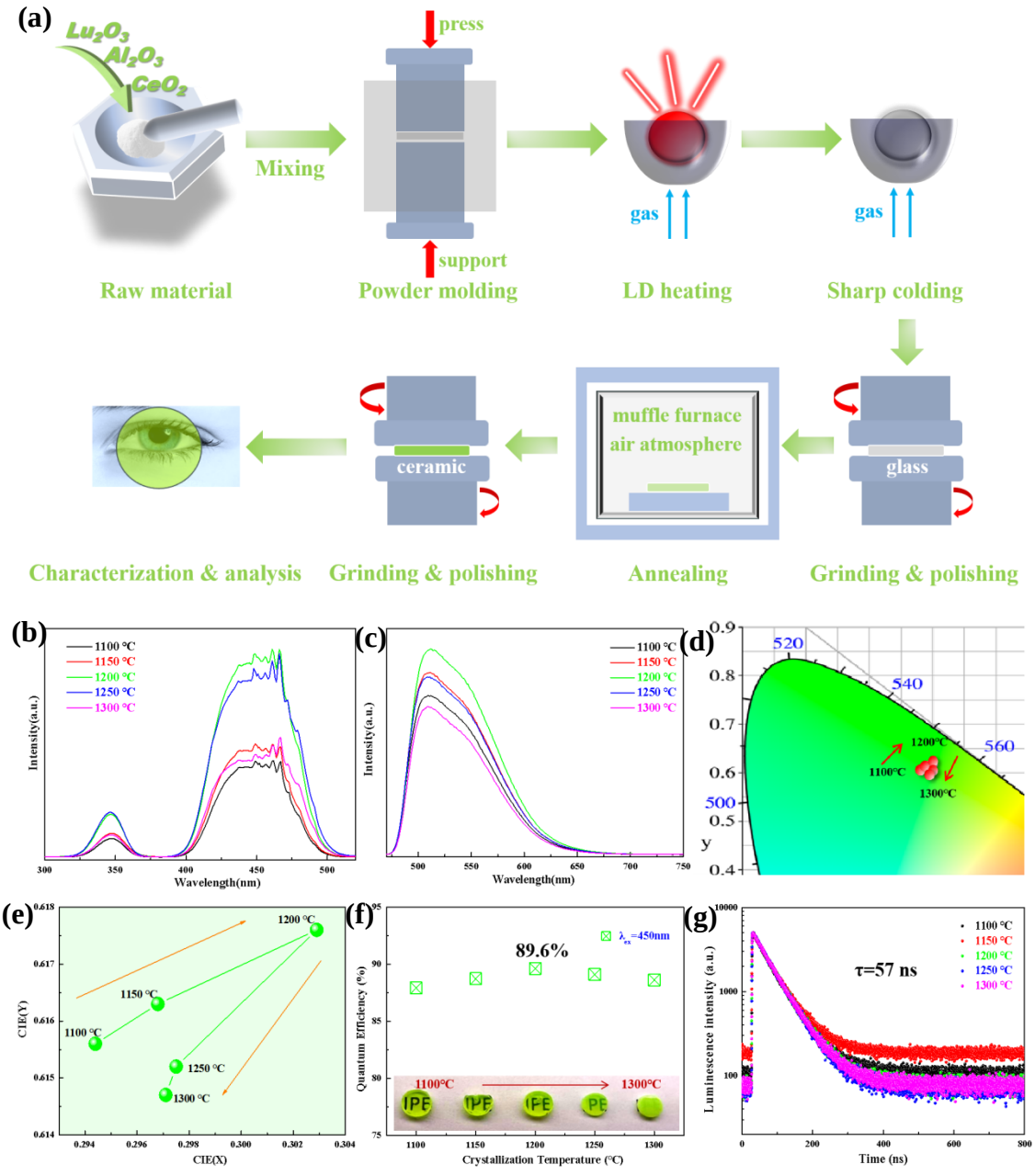

Figure 1. (a) Flowchart of the preparation of transparent Ce:LuAG-Al_2O_3 nanoceramics, (b) PLE spectra, (c) PL spectra, (d) CIE color coordinates, (e) plot of numerical changes in color coordinates, (f) QE (the images of nanoceramics crystallized at different temperatures are indicated in the bottom inset), (g) fluorescent decay curves of transparent Ce:LuAG-Al_2O_3 nanoceramics crystallized at different temperatures.

Figure 2(a) shows the XRPD patterns of transparent nanoceramics crystallized at different temperatures. It can be seen that the diffraction peak intensity gradually

increases with the improvement of crystallization temperature, indicating a more complete crystal development. The in-line transmittance of transparent nanoceramics crystallized at different temperatures is presented in **Figure 2(b)**. With the increase of crystallization temperature, the optical transmittance of transparent nanoceramics first increases and then decreases. When the crystallization temperature is 1300 ℃, the transparent nanoceramics become completely opaque. SEM images of the nanoceramics crystallized at different temperatures are presented in **Figure 2(c).** The grain size gradually increases with the raise of crystallization temperature (**Figure S2**). It can also be seen that there are two types of crystalline phases in the crystal. In addition to the main LuAG phase (bright contrast), there is also an in situ-generated secondary Al_2O_3 phase (dark contrast), which is confirmed by **Figure 3** and **Figure S3**. According to the XRPD results, the transparent nanoceramics are composed of 86.03 wt% LuAG garnet phase and 13.97 wt% Al_2O_3 phase. Due to the large difference in refractive index between main LuAG phase (~1.84) and secondary Al_2O_3 phase (~1.76),[47] as the grain size gradually increases, the scattering effect on visible light becomes more significant, leading to a deterioration in the optical transmittance of nanoceramics.

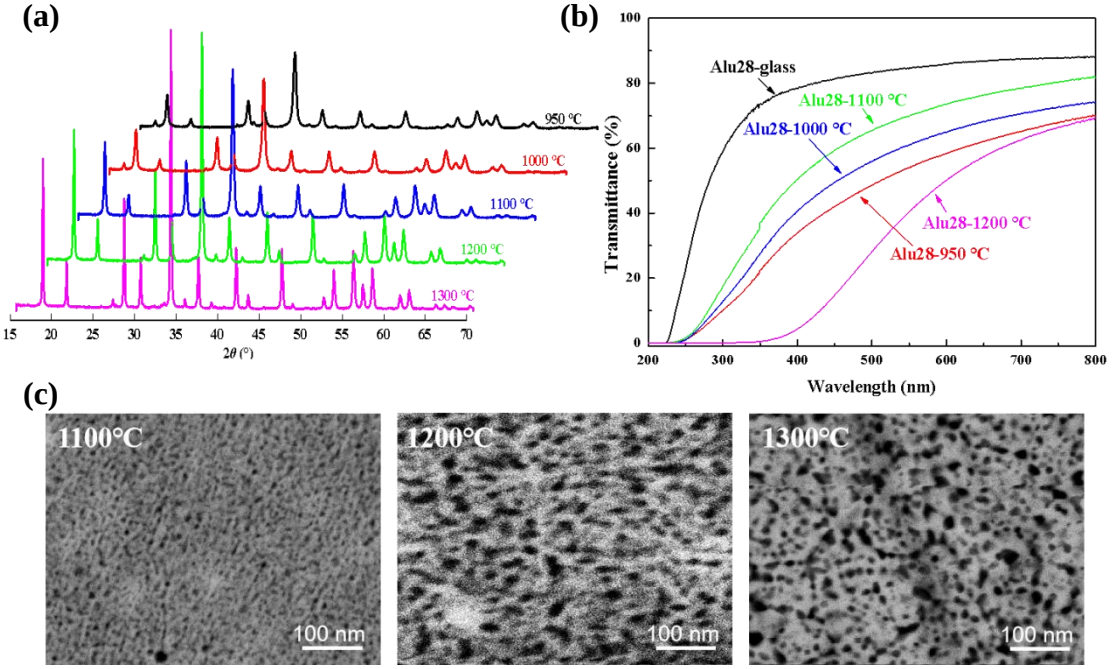

Figure 2. (a) XRPD patterns, (b) in-line transmittance, (c) SEM patterns of transparent LuAG-Al_2O_3 nanoceramics crystallized at different temperatures.

Figure 3(a) shows the STEM-HAADF image of transparent Ce:LuAG-Al_2O_3 nanoceramics crystallized at 1200 ℃. It can be seen that there are two phases with different brightness. The continuous uniform bright region is the main LuAG phase with the higher average atomic number ($\overline{Z_{LuAG}} \approx 47.6$), the granular and elliptical dark region is the in situ-generated secondary Al_2O_3 phase with a lower average atomic number ($\overline{Z_{Al2O3}} \approx 10.6$). The Al_2O_3 phase stands within the LuAG phase, i.e. intragranular Al_2O_3. Another elliptical Al_2O_3 phase with larger areas can be observed between the LuAG grains, i.e. intergranular Al_2O_3. **Figure 3(b)** shows a typical HRTEM image of transparent Ce:LuAG-Al_2O_3 nanoceramics and **Figure 3(c-e)** are the corresponding fast Fourier transform (FFT) patterns of the different regions. **Figure 3(c)** indicates that the continuous uniform dark region (1) is LuAG phase, and **Figure 3(d,e)** show that the granular and elliptical bright regions (2,3) match well with θ-Al_2O_3 phase. The STEM-HAADF micrograph and EDX line-scan results of transparent Ce:LuAG-Al_2O_3 nanoceramics are presented in **Figure 3(f)**. For the continuous uniform bright region, the proportions of Lu and Al elements are approximately 38% and 62%, which is in very good agreement with the ratio of Lu (37.5%) and Al (62.5%) of the LuAG phase. The ratio of Al element in the elliptical dark region is 100%, and there are no Lu element present. Therefore, it is obvious that the continuous uniform bright region is mainly LuAG phase and the elliptical dark region is mainly Al_2O_3 phase. A small amount of Ce element has also been detected, however it is difficult to accurately determine the ratio of Ce in the different regions due to its small content. **Figure 3(g)** shows a STEM-HAADF image of transparent Ce:LuAG-Al_2O_3 nanoceramics and **Figure 3(h-j)** are the corresponding EDS elemental maps. The Lu element exists in the area outside the elliptical dark region, and the Al element is distributed throughout the entire area, but there is enrichment in the elliptical dark region, which is also confirmed by **Figure S4**. Although the content of Ce element is very low, it can still be observed from **Figure 3(j)** that the Ce element is localized in the LuAG phase and that no segregation appears at the grain boundaries. These results also indicate that the continuous uniform bright region is

mainly LuAG phase and the elliptical dark region is Al_2O_3 phase. Therefore, the prepared transparent Ce:LuAG-Al_2O_3 nanoceramics have a three-dimensional network structure composed of main LuAG phase and in situ-generated secondary Al_2O_3 phase.

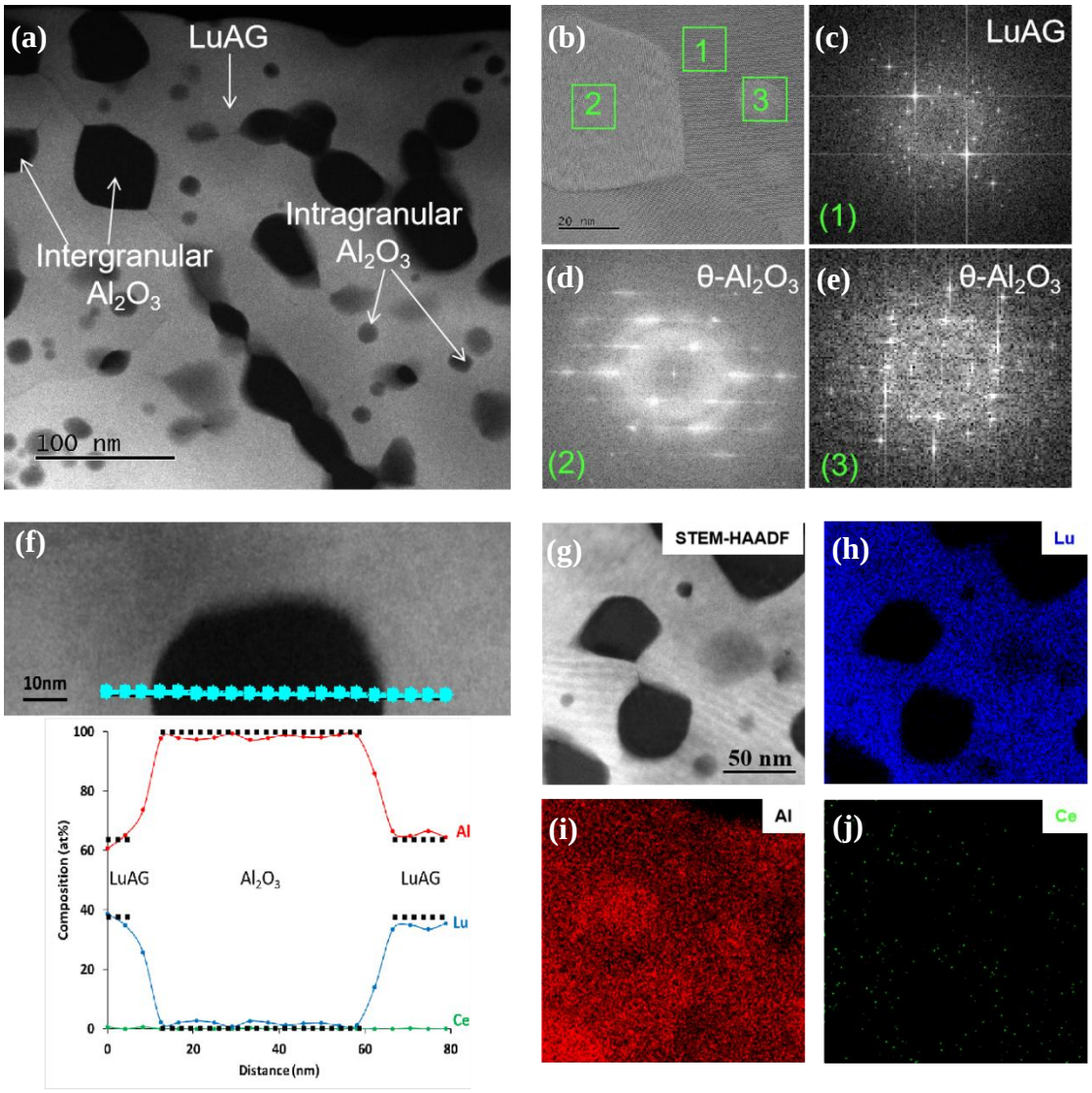

Figure 3. (a) STEM-HAADF image, (b) HRTEM image, (c-e) fast Fourier transform (FFT) patterns, (f) STEM-HAADF micrograph and EDX line-scan results, (g-j) the corresponding STEM-HAADF image and EDS elemental maps of Lu (blue), Al (red) and Ce (green) of transparent Ce:LuAG-Al_2O_3 nanoceramics (1200 ℃).

Figure 4(a) shows the PL intensity of transparent 0.3%Ce:LuAG-Al_2O_3 nanoceramics crystallized at 1200 ℃ and transparent 0.3%Ce:LuAG ceramics as a function of temperature. The PL intensity of the two ceramic materials gradually

decrease with the increase of temperature. Compared to its value at room temperature , the PL intensity of transparent 0.3%Ce:LuAG-Al_2O_3 nanoceramics only decreases by 2.9% at 200 ℃, while a 4.5% PL intensity decrease is observed for transparent 0.3%Ce:LuAG ceramics. **Figure 4(b)** is the contour plot of thermal quenching behaviors of transparent 0.3%Ce:LuAG-Al_2O_3 nanoceramics crystallized at 1200 ℃ in the 25-300 ℃ temperature range. It can be seen that the integrated luminous intensity of the transparent 0.3%Ce:LuAG-Al_2O_3 nanoceramics remains at a high level (>90% of RT) with the increase of temperature, even when the temperature reaches 300 ℃. The effect of temperature on the quantum efficiency (QE) of transparent 0.3%Ce:LuAG-Al_2O_3 nanoceramic crystallized at 1200 ℃ under the excitation of 450 nm wavelength blue light is shown in **Figure 4(c)**. The quantum efficiency of transparent 0.3%Ce:LuAG-Al_2O_3 nanoceramics decreases with the increase of temperature. However, when the temperature reaches 200 °C, the quantum efficiency still remains at 97.4% of its value at room temperature. These results indicate that the transparent 0.3%Ce:LuAG-Al_2O_3 nanoceramics possess good thermal stability and can maintain good luminous intensity and luminous efficiency at high temperature (~200 °C). The presence of in situ-generated secondary Al_2O_3 phase improves the thermal conductivity and reduces operating temperature of the nanoceramics, thereby improving the thermal stability of the nanoceramics. Kang et al.[49] studied the thermal stability of Ce:YAG ceramics containing different contents of Al_2O_3 under high-power LD excitation, and found that when the Al_2O_3 content exceeds 20%, the performance of Ce:YAG ceramics was significantly improved. Good thermal stability enable transparent Ce:LuAG-Al_2O_3 nanoceramics to be used for high-power LD and to achieve high brightness green lighting.

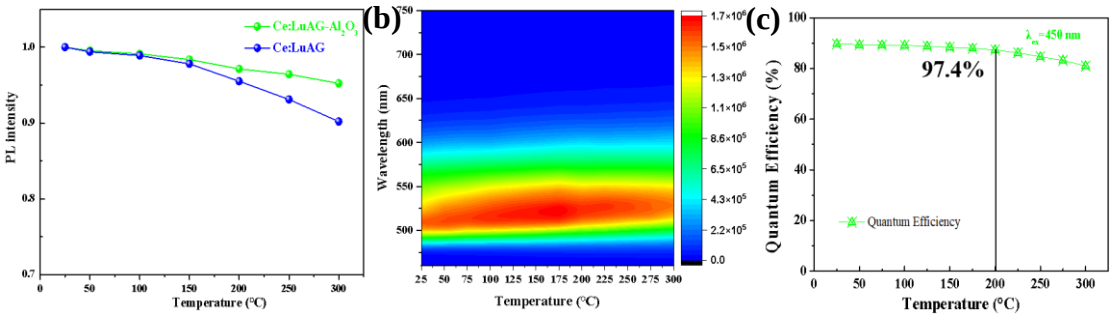

Figure 4. (a) PL intensity of transparent 0.3%Ce:LuAG-Al_2O_3 nanoceramics (1200 ℃) and transparent 0.3%Ce:LuAG ceramics varies with temperature, (b) contour plot of thermal quenching behaviors and (c) QE of transparent 0.3%Ce:LuAG-Al_2O_3 nanoceramics (1200 ℃) varies with temperature.

Figure 5 shows laser scanning confocal images of transparent 0.3%Ce:LuAG ceramics and transparent 0.3%Ce:LuAG-Al_2O_3 nanoceramics crystallized at 1200 ℃. These are used to analyze light scattering properties of the two ceramic samples. Under 470 nm laser irradiation, a brighter and clearer surface can be seen, which is evidenced by the two-dimensional (2D) and three-dimensional (3D) images in **Figure 5(a-d)**. It can be seen from **Figure 5(a,b)** that there are some large bright spots in the 0.3%Ce:LuAG ceramics. These can be assigned to different luminescence intensities between the grain and the grain boundary. Thereby, the uniformity of the distribution of luminescent centers in 0.3%Ce:LuAG ceramics needs to be improved. Transparent 0.3%Ce:LuAG-Al_2O_3 nanoceramics have smaller grain size and in-situ generated Al_2O_3 second phase. The large refractive index difference between the main LuAG phase and in situ-generated secondary Al_2O_3 phase causes significant light scattering effect. Meanwhile, the larger secondary Al_2O_3 phase can also serve as the scattering center to enhance the scattering effect of incident light. Therefore, transparent 0.3%Ce:LuAG-Al_2O_3 nanoceramics have better scattering effect and absorption efficiency for incident blue laser. As shown in **Figure 5(c,d)**, compared to 0.3%Ce:LuAG ceramics, transparent 0.3%Ce:LuAG-Al_2O_3 nanoceramics exhibit more uniform luminescent centers. **Figure 5(e,f)** show light beam photographs of transparent 0.3%Ce:LuAG-Al_2O_3 nanoceramics and 0.3%Ce:LuAG ceramics driven by blue LD (4.5 W). From the light beam photographs, it can be seen that the 0.3%Ce:LuAG ceramics demonstrate insufficient scattering effect on blue LD light, resulting in blue LD light directly passing through them and generating transmitted blue dot. In contrast, transparent 0.3%Ce:LuAG-Al_2O_3 nanoceramics generate more uniform and bright green light due to their more effective scattering and absorption of blue LD light, avoiding the transmitted blue dot problem during LD driven lighting.

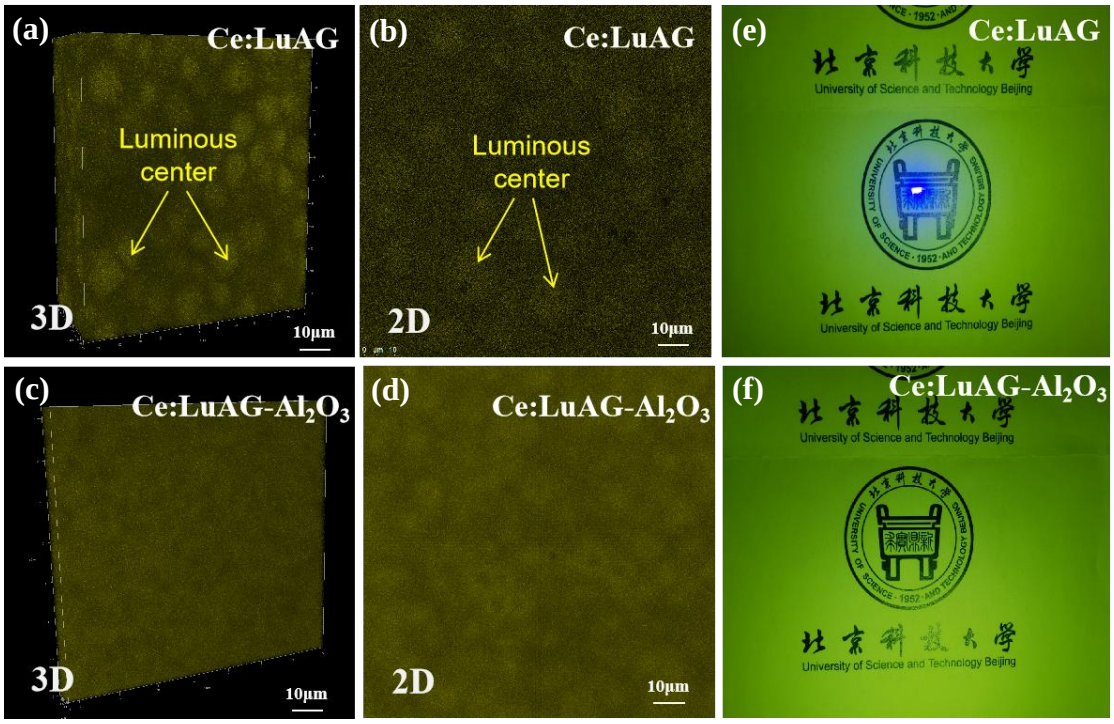

Figure 5. (a-d) Laser scanning confocal images of transparent 0.3%Ce:LuAG ceramics and 0.3%Ce:LuAG-Al_2O_3 nanoceramics (1200 ℃), (e-f) corresponding LD-driven light beam photographs (recorded in transmission mode).

In order to study the luminescence properties of transparent 0.3%Ce:LuAG-Al_2O_3 nanoceramics for LD lighting, ceramic sheets with a diameter of 10 mm and a thickness of 1.0 mm were combined with a blue LD (450 nm) to make a LD lighting device. **Figure 6(a)** is the schematic diagram of LD lighting device analysis system. **Figure 6(b)** shows the electroluminescence (EL) spectra of transparent 0.3%Ce:LuAG-Al_2O_3 nanoceramics crystallized at different temperatures under the excitation of blue LD. The green light emission intensity of transparent 0.3%Ce:LuAG-Al_2O_3 nanoceramics reaches maximum value when the crystallization temperature is 1200 ℃. The absorption efficiency (Abs.), internal efficiency (IE) and luminous efficiency (LE) of transparent 0.3%Ce:LuAG-Al_2O_3 nanoceramics crystallized at different temperatures are shown in **Figure 6(c)**. The absorption efficiency of transparent 0.3%Ce:LuAG-Al_2O_3 nanoceramics first increases and then decreases with the increase of crystallization temperature, and reaches its maximum value at 1200 ℃. As the crystallization temperature increases, both the main LuAG

phase and the in situ-generated secondary Al_2O_3 phase in nanoceramics develop more perfectly. The scattering and absorption effects of incident blue laser are more significant. However, when the crystallization temperature exceeds 1200 ℃, the transmittance of the nanoceramics significantly decreases, resulting in the inability of the incident blue laser to effectively enter inside the nanoceramics, resulting in a decrease in absorption efficiency. The internal efficiency (IE) and luminous efficiency (LE) of transparent nanoceramics gradually increase with the improvement of crystallization temperature. The maximum values of internal efficiency (IE) and luminous efficiency (LE) are 68.5% and 281.6 $lm \cdot W^{-1}$, respectively. When the crystallization temperature is 1200 ℃, the internal efficiency (IE) and luminous efficiency (LE) of nanoceramics are 62.3% and 257.2 $lm \cdot W^{-1}$, respectively. Compared with the current luminous efficiency of Ce:LuAG (~200 $lm \cdot W^{-1}$), there is a significant improvement of transparent 0.3%Ce:LuAG-Al_2O_3 nanoceramics. **Figure 6(d)** shows the color coordinates and corresponding luminescent images of transparent 0.3%Ce:LuAG-Al_2O_3 nanoceramics crystallized at different temperatures in the standard of CIE 1931. As the crystallization temperature increases, the color coordinate of the transparent 0.3%Ce:LuAG-Al_2O_3 nanoceramics moves towards the edge of the CIE diagram, indicating the improvement of color saturability (color purity).[47] The color coordinates of the transparent nanoceramics crystallized at 1200 ℃ are (0.30, 0.53). When the crystallization temperature increases above 1200 ℃, the color coordinates of transparent nanoceramics are very similar.

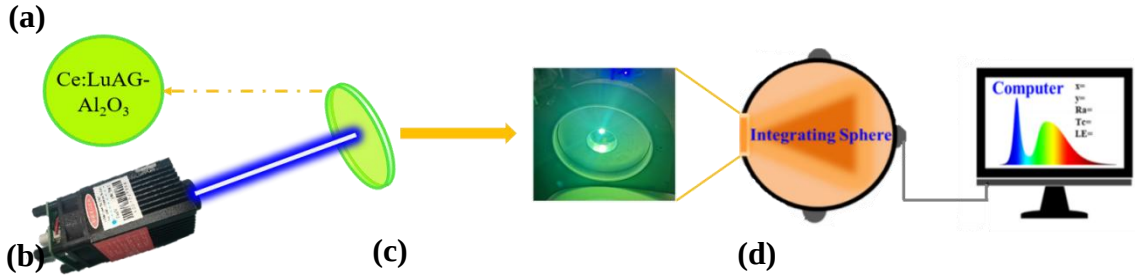

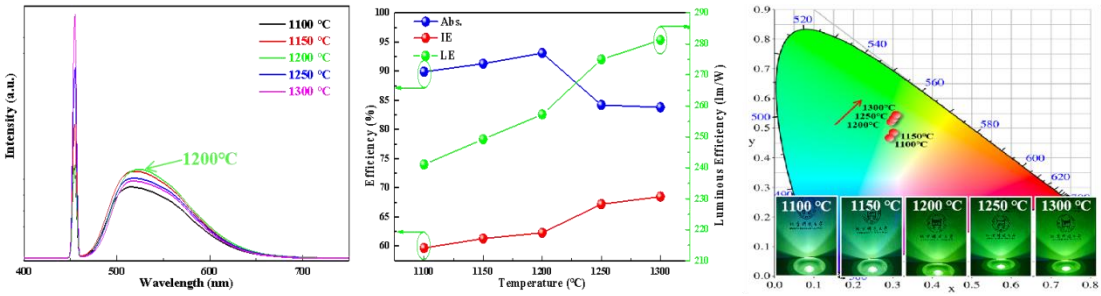

Figure 6. (a) Schematic diagram of LD lighting device analysis system, (b) EL spectra, (c) absorption efficiency (Abs.), internal efficiency (IE) and luminous efficiency (LE), (d) color coordinates of transparent 0.3%Ce:LuAG-Al_2O_3 nanoceramics crystallized at different temperatures. The incident laser power density is 5 W·mm^{-2}. The corresponding luminescent images are indicated in the right inset.

Figure 7(a) shows the normalized EL spectra of transparent 0.3%Ce:LuAG-Al_2O_3 nanoceramics crystallized at 1200 ℃ under different laser power densities. It can be seen that the PL spectrum of transparent nanoceramics only shows a very slight shift with the increase of laser power density, which ensures luminescence stability at high power density. The corresponding CIE chromaticity coordinates of transparent 0.3%Ce:LuAG-Al_2O_3 nanoceramics with increasing laser power density presented in **Figure 7(b)** also confirm this point. The x and y values of transparent 0.3%Ce:LuAG-Al_2O_3 nanoceramics hardly change with the gradual increase of laser power density. **Figure 7(c)** presents the luminous flux (LF) and luminous efficiency (LE) of transparent 0.3%Ce:LuAG-Al_2O_3 nanoceramics (1200 ℃) and 0.3%Ce:LuAG ceramics with increasing laser power density. The LF of transparent 0.3%Ce:LuAG-Al_2O_3 nanoceramics and transparent 0.3%Ce:LuAG ceramics exhibit the same trend, i.e. gradual increase with the improvement of laser power density. They eventually reach the inflection point and slow down the rate of increase. When the laser power density is 10.9 W·mm^{-2}, the LF of transparent 0.3%Ce:LuAG ceramics reaches a maximum of 844.5 lm. However, when the transparent 0.3%Ce:LuAG-Al_2O_3 nanoceramics are excited by blue laser, an extremely high LF of 5125 lm is achieved and the laser power density is 29.83 W·mm^{-2}. The LE of transparent 0.3%Ce:LuAG-Al_2O_3 nanoceramics and transparent

0.3%Ce:LuAG ceramics first increases and then decreases. The maximum LE of transparent 0.3%Ce:LuAG ceramics and transparent 0.3%Ce:LuAG-Al_2O_3 nanoceramics are 169.4 lm·W^{-1} and 247.9 lm·W^{-1}, respectively. **Table 1** summarizes the luminescent properties of various color converters under excitation of blue laser. Compared to the reported color converters, the LF and LE of transparent Ce:LuAG-Al_2O_3 nanoceramics are almost the best results so far. The luminous density of transparent 0.3%Ce:LuAG-Al_2O_3 nanoceramics can reach up to 4235.5 lm·mm^{-2}. From these results, the transparent Ce:LuAG-Al_2O_3 nanoceramics elaborated in this paper demonstrate an extremely high LF of 5125 lm, a good luminous density of 4235.5 lm·mm^{-2} and a maximum LE of 247.9 lm·W^{-1}. Therefore these transparent Ce:LuAG-Al_2O_3 nanoceramics are believed to be promising green color converters for high-brightness LD lighting.

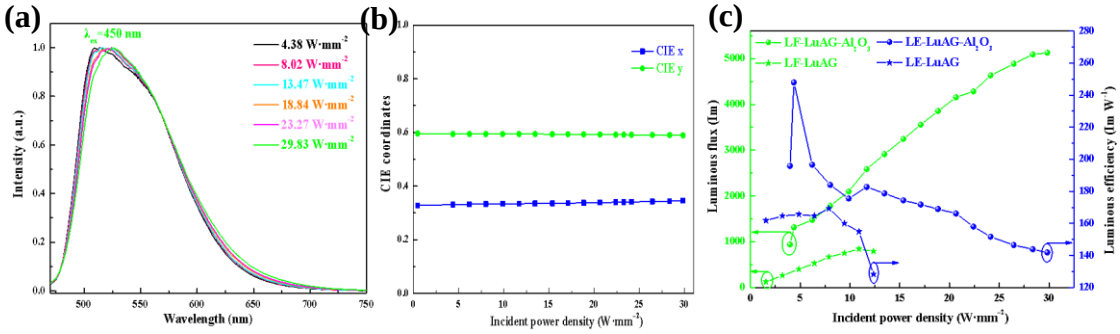

Figure 7. (a) Normalized EL spectra and (b) CIE chromaticity coordinates of transparent 0.3%Ce:LuAG-Al_2O_3 nanoceramics (1200 ℃), (c) luminous flux (LF) and luminous efficiency (LE) of transparent 0.3%Ce:LuAG-Al_2O_3 nanoceramics (1200 ℃) and 0.3%Ce:LuAG ceramics under the different laser power density.

Table 1. Luminescent properties of various color converters under excitation of blue laser

	Luminous flux (lm)	Luminous efficiency (lm·W^{-1})	Lumen density (lm·mm^{-2})
YAG TC	~525	223	/
YAG SC	1618	105.5	/
YAG-Al_2O_3 CCP	1367	135.3	2719.6
LuAG TC	844	154.8	1679.6
LuAG-Al_2O_3 CCP	3081	216	6129

This work	**5125**	**142.0**	**4235.5**

4. Conclusions

In the present study, we have successfully prepared a new type of transparent Ce:LuAG-Al_2O_3 nanoceramic with an excessive Al_2O_3 component design strategy via a bulk glass-crystallization method. The resulting transparent Ce:LuAG-Al_2O_3 nanoceramics present a biphasic three-dimensional network nanostructure, in which the in-situ generated Al_2O_3 secondary phase improve the thermal stability of the ceramic and serve as scattering centers to enhance the absorption and conversion efficiency of incident blue laser and the uniformity of emitting green light. The PL intensity and quantum efficiency of transparent Ce:LuAG-Al_2O_3 nanoceramics crystallized at 1200 ℃ only decrease by 2.9% and 2.6% respectively at 200 ℃. Under the excitation of blue laser (5 $W \cdot mm^{-2}$), the maximum internal efficiency (IE) and luminous efficiency (LE) of transparent Ce:LuAG-Al_2O_3 nanoceramic (1300 ℃) are 68.5% and 281.6 $lm \cdot W^{-1}$, respectively. More importantly, when the laser power density is 29.83 $W \cdot mm^{-2}$, the maximum luminous flux reaches 5125 lm and the maximum luminous density reaches 4235.5 $lm \cdot mm^{-2}$, which is almost the best performance of transparent Ce:LuAG ceramics in LD lighting to date. A maximum luminous efficiency of 247.9 $lm \cdot W^{-1}$ is also obtained under the laser excitation of 4.38 $W \cdot mm^{-2}$. It is believed that the transparent Ce:LuAG-Al_2O_3 nanoceramics prepared in this paper are promising green-emitting color converters for high power LD-driven high brightness solid-state lighting. The excessive Al_2O_3 components design strategy should stimulate further research to approach high performance garnet-based transparent ceramics in the field of high-power LD lighting.

Supporting Information

Supporting Information is available from the Wiley Online Library or from the author.

Acknowledgement

This work is financially supported by the National Natural Science Foundation of China (NSFC No. 51972304), the Project of Scientific Experiment on Chinese Manned Space Station, Chinese Academy of Sciences President's International

Fellowship Initiative for 2021 (No. 2021VEA0012), and the Fundamental Research Funds for the Central Universities.

Conflict of Interest

The authors declare no conflict of interest.

Data Availability Statement

The data that support the findings of this study are available from the corresponding author upon reasonable request.

Keywords

Transparent ceramics, Ce:LuAG-Al_2O_3 phosphor ceramics, Nanoceramics, LD lighting

References

[1] E. F. Schubert, J. K. Kim, *Science* **2005**, *308*, 1274.

[2] J. M. Gee, J. Y. Tsao, J. A. Simmons, *Nat. Photonics* **2004**, *3*, 180.

[3] P. Pust, P. J. Schmidt, W. Schnick, *Nat. Mater*. **2015**, *14*, 454.

[4] M. Zhao, H. Liao, M. S. Molokeev, Y. Zhou, Q. Zhang, Q. Liu, Z. Xia, *Light Sci. Appl.* **2019**, *8*, 9.

[5] M. H. Crawford, *IEEE J. Sel. Top. Quant*. **2009**, *15*, 1028.

[6] H. Ding, Z. Liu, P. Hu, Y. Liu, J. Jiang, *Adv. Opt. Mater.* **2021**, *9*, 2002141.

[7] A. Neumann, J. J. Wierer, W. Davis, Y. Ohno, S. R. J. Brueck, J. Y. Tsao, *Opt. Express* **2011**, *19*, A982.

[8] Q. Yao, P. Hu, P. Sun, M. Liu, R. Dong, K. F. Chao, Y. F. Liu, J. Jiang, H. C. Jiang, *Adv. Mater*. **2020**, *32*, 1907888.

[9] Q. X. Wen, Y. Wang, C. Zhao, L. Xu, X. D. Wang, Y. S. Xu, S. Lin, X. J. Liang, J. P. Liu, W. D. Xiang, *Laser Photon. Rev*. **2023**, *7*, 963.

[10] Y. R. Xu, S. X. Li, P. Zheng, L. Wang, S. H. You, T. Takeda, N. Hirosaki, R. J. Xie, *J. Mater. Chem. C.* **2019**, *7*, 11449.

[11] S. You, S. X. Li, L. Wang, T. Takeda, N. Hirosaki, R. J. Xie, *Chem. Eng. J*. **2021**, *404*, 126575.

[12] Q. Q. Zhu, X. J. Wang, L. Wang, N. Hirosaki, T. Nishimura, Z. F. Tian, Q. Li, Y. Z. Xu, X. Xu, R. J. Xie, *J. Mater. Chem. C*. **2015**, *3*, 10761.

[13] S. Liu, P. Sun, Y. Liu, T. Zhou, S. X. Li, R. J. Xie, X. Xu, R. Dong, J. Jiang, H. Jiang, *ACS Appl. Mater. Interfaces* **2019**, *11*, 2130.

[14] L. Wang, R. J. Xie, Y. Li, X. Wang, C. G. Ma, D. Luo, T. Takeda, Y. T. Tsai, R. S. Liu, N. Hirosaki, *Light: Sci. Appl*. **2016**, *5*, 16155.

[15] P. Sun, P. Hu, Y. Liu, S. Liu, R. Dong, J. Jiang, H. Jiang, *J. Mater. Chem. C* **2020**, *8*, 1405.

[16] J. Sun, H. Lin, D. W. Zhang, R. J. Hong, C. X. Tao, Z. X. Han, *Ceram. Int*. **2019**, *45*, 23643.

[17] Y. H. Kim, P. Arunkumar, B. Y. Kim, S. Unithrattil, E. Kim, S. H. Moon, J. Y. Hyun, K. H. Kim, D. Lee, J. S. Lee, W. B. Im, *Nat. Mater*. **2017**, *16*, 543.

[18] J. Park, S. Cho, H. Kwon, *Sci. Rep*. **2018**, *8*, 17852.

[19] Y. Ma, W. Lan, B. Xie, R. Hu, X. Luo, *Int. J. Heat Mass Transf*. **2018**, *116*, 694.

[20] E. Kim, H. W. Shim, S. Unithrattil, Y. H. Kim, H. Choi, K. J. Ahn, J. S. Kwak, S. Kim, H. Yoon, W. B. Im, *ACS Nano* **2016**, *10*, 238.

[21] J. Yu, S. Si, Y. Liu, X. Zhang, Y. Cho, Z. Tian, R. Xie, H. Zhang, Y. Li, J. Wang, *J. Mater. Chem. C* **2018**, *6*, 8212.

[22] H. Lin, T. Hu, Y. Cheng, M. Chen, Y. Wang, *Laser Photon. Rev*. **2018**, *12*, 1700344.

[23] X. Y. Li, C. B. Yang, L. T. Qiu, S. X. Wang, Y. H. Chen, M. Yin, D. Q. Chen, *Laser Photon. Rev*. **2021**, *16*, 2100346.

[24] M. H. Balci, F. Chen, A. B. Cunbul, O. Svensen, M. N. Akram, X. Chen, *Opt. Rev*. **2017**, *25*, 166.

[25] J. Xu, A. Thorseth, C. Xu, A. Krasnoshchoka, M. Rosendal, C. Dam-Hansen, B. Du, Y. Gong, O.B. Jensen, *J. Lumin*. **2019**, *212*, 279.

[26] Y. Yuan, D. Wang, B. Zhou, S. Feng, M. Sun, S. Zhang, W. Gao, Y. Bi, H. Qin,

Opt. Mater. Express **2018**, *8*, 2760

[27] Z. Y. Yang, T. D. Boer, P. M. Braun, B. B. Su, Q. Y. Zhang, A. Moewes, Z. G. Xia, *Adv. Mater*. **2023**, *35*, 2301837.

[28] S. W. Feng, Y. C. Guo, M. Allix, S. X. Li, R. J. Xie, J. Fu, C. Genevois, E. Véron, H. Wang, Y. F. Yang, H. M. Qin, J. Q. Li, *Cell Rep Physi Sci*. **2022**, *3*, 101044.

[29] S. X. Li, L. Wang, N. Hirosaki, R. J. Xie, *Laser Photon. Rev*. **2018**, *12*, 1800173.

[30] C. Y. Ma, Y. G. Cao, *Appl. Phys. Lett*. **2021**, *118*, 210503.

[31] J. F. Lin, Y. Zhou, Q. L. Lu, X. Wu, C. Lin, T. F. Lin, K. H. Xue, X. S. Miao, B. S. Sa, Z. M. Sun, *J. Mater. Chem. A* **2019**, *7*, 19374.

[32] X. Wu, J. F. Lin, Z. Xu, C. L. Zhao, C. Lin, H. J. Wang, T. F. Lin, X. H. Zheng, B. S. Sa, Q. W. Zhang, K. Wang, Z. M. Sun, J. W. Zhai, *Laser Photon. Rev*. **2021**, *15*, 2100211.

[33] Z. Wang, G. Zhou, D. Jiang, S. Wang, *J. Adv. Ceram*. **2018**, *7*, 289.

[34] J. R. Ling, Y. F. Zhou, W. T. Xu, H. Lin, S. Lu, B. Wang, K. Wang, *J. Adv. Ceram*. **2020**, *9*, 45-54.

[35] A. C. Berends, M. A. Haar, M. R. Krames, *Chem. Rev*. **2020**, *120*, 13461.

[36] S. Hu, X. P. Qin, G. H. Zhou, C. H. Lu, G. H. Liu, Z. Z. Xu, S. W. Wang, *Opt. Mater. Express* **2015**, *5*, 2902.

[37] J. Xu, J. Wang, Y. X. Gong, X. F. Ruan, Z. W. Liu, B. F. Hu, B. G. Liu, H. Li, X. L. Wang, B. L. Du, *J. Eur. Ceram. Soc*. **2018**, *38*, 343.

[38] K. Li, Y. Shi, F. Q. Jia, C. Price, Y. K. Gong, J. G. Huang, N. Copner, H. Cao, L. Z. Yang, S. Chen, H. H. Chen, J. Li, *IEEE Photonic. Tech. L*. **2018**, *30*, 939.

[39] C. Gu, X. J. Wang, C. Xia, S. X. Li, P. Liu, D. Li, H. Li, G. Zhou, J. Zhang, R. J. Xie, *J. Mater. Chem. C* **2019**, *7*, 8569.

[40] X. Liu, X. L. Qian, P. Zheng, Z. W. Hu, X. P. Chen, H. M. Pan, J. Zou, R. J. Xie, J. L, *J. Eur. Ceram. Soc.* **2019**, *39*, 4965.

[41] X. L. Peng, S. X. Li, Z. H. Liu, B. H. Zhang, Y. S. Peng, D. Yu, R. D. Tian, X. M.

Yao, Z. R. Huang, X. J. Liu, R. J. Xie, *J. Eur. Ceram. Soc*. **2021**, *41*, 5650.

[42] Z. H. Liu, S. X. Li, Y. H. Huang, L. J. Wang, Y. R. Yao, T. Long, X. M. Yao, X. J. Liu, Z. R. Huang, *Ceram. Int*. **2018**, *44*, 20232.

[43] X. G. Ma, X. Y. Li, J. Q. Li, C. Genevois, B. Q. Ma, A. Etienne, C. L. Wan, E. Véron, Z. J. Peng, M. Allix, *Nat Commun*. **2018**, *9*, 1175.

[44] J. L. Wu, G. Gundiah, A. K. Cheetham, *Chem. Phys. Lett*. **2007**, *441*, 250.

[45] H. Y. Dong, S. Y. Tian, X. J. Sun, I. S. Mukhin, R. M. Islamova, G. Li, J. J. Tian, *Adv. Optical Mater*. **2023**, *11*, 2300309.

[46] J. Xu, D. A. Hassan, R. J. Zeng, D. L. Peng, *J. Eur. Ceram. Soc*. **2016**, *36*, 2017.

[47] Q. Zhang, R. L. Zheng, J. Y. Ding, P. Cui, Z. Y. Wang, P. Lv, W. Wei, *J. Am. Ceram. Soc*. **2021**, *104*, 3260.

[48] C. Y. Ma, F. Tang, J. D. Chen, R. Ma, X. Y. Yuan, Z. C. Wen, J. Q. Long, J. T. Li, M. M. Du, J. T. Zhang, Y. G. Cao, *J. Eur. Ceram. Soc*. **2016**, *36*, 4205.

[49] T. Kang, S. Lee, J. Kim, Y. Jeong, J. Park, *J. Lumin*. **2020**, *222*, 117077.

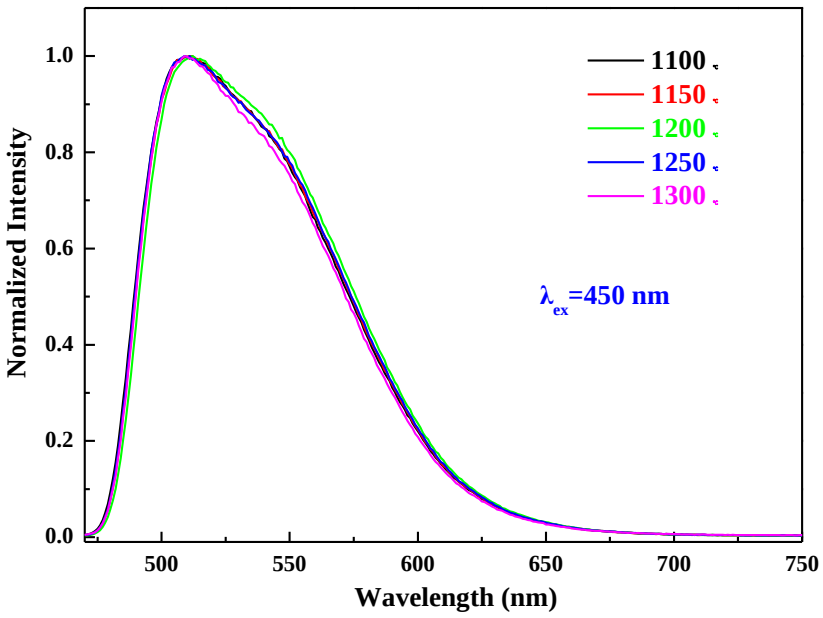

Figure S1. Normalized photoluminescence emission (PL) spectra (λ_{ex}=450 nm) of the transparent 0.3%Ce:LuAG-Al_2O_3 nanoceramics crystallized at 1200 ℃.

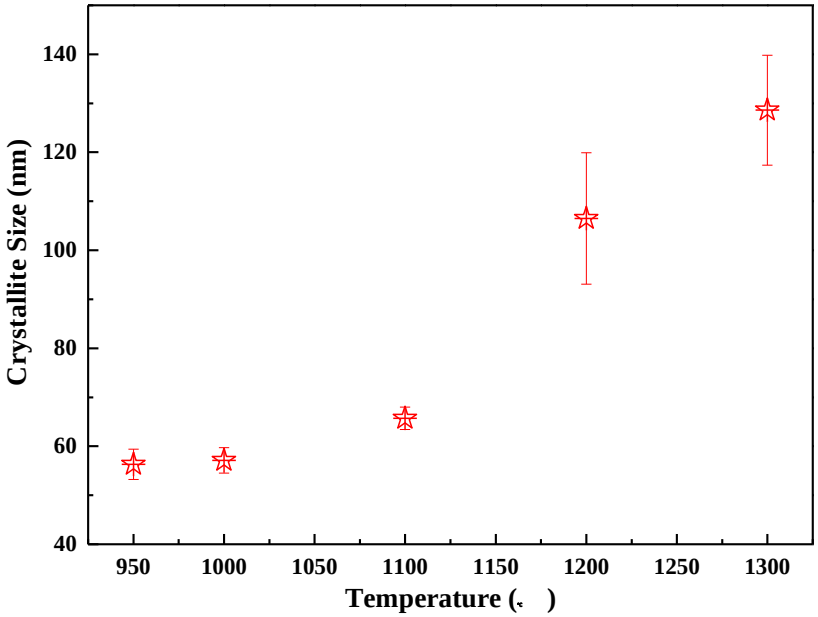

Figure S2. The crystallite sizes of the transparent 0.3%Ce:LuAG-Al_2O_3 nanoceramics crystallized at different temperatures.

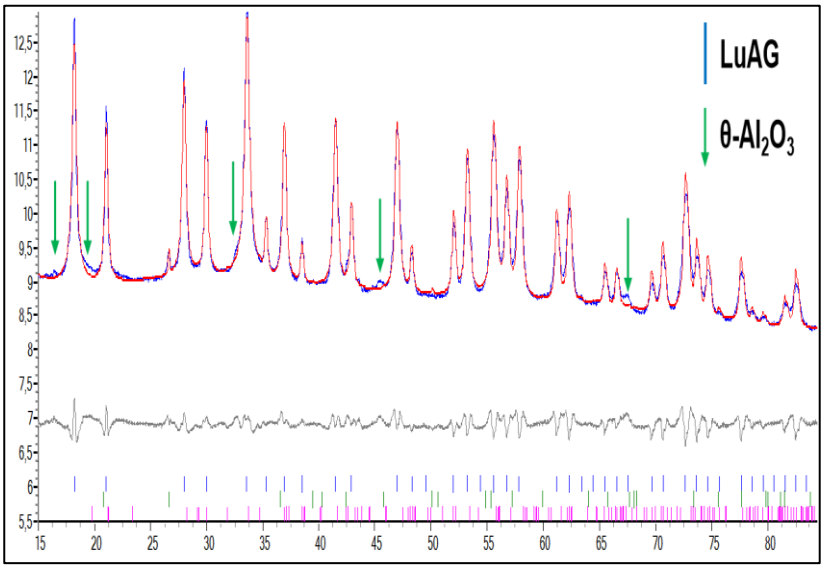

Figure S3. High-resolution X-ray powder diffraction (HR-XRPD) pattern of the transparent 0.3%Ce:LuAG-Al_2O_3 nanoceramics crystallized at 1200 ℃.

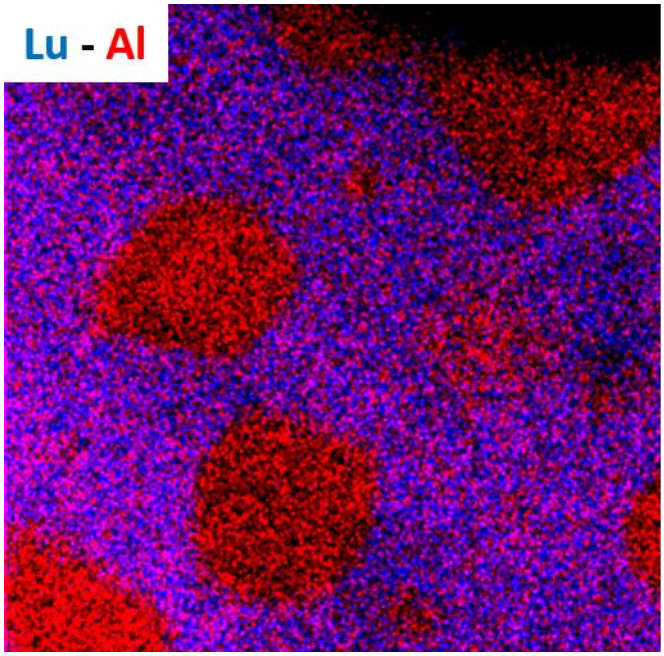

Figure S4. EDS elemental maps of Lu and Al (blue and red) of transparent Ce:LuAG-Al_2O_3 nanoceramics crystallized at 1200 ℃.